Available online at www.sciencedirect.com
ScienceDirect
Journal of Sound and Vibration 307 (2007) 349–364
JOURNAL OF SOUND AND VIBRATION
www.elsevier.com/locate/jsvi

Damping estimation via energy-dissipation method

Jin-Wei Liang*

Department of Mechanical Engineering, Mingchi University of Technology, 84 Gung-Juan Rd., Taishan, Taipei County, Taiwan

Received 6 June 2006; received in revised form 27 June 2007; accepted 11 July 2007

Abstract

This paper extends an existing single-degree-of-freedom (dof) energy-dissipation scheme to identify damping parameters for multiple-dof vibration systems. The method balances the energy input of the real system against the energy dissipated in a theoretical model to develop the identification algorithms. The theoretical friction model is assumed to consist of the viscous and Coulomb damping components. The proposed algorithms are applicable in the general- and periodic-input cases. According to the numerical studies performed on periodic excitation, the mixed-frequency harmonic input is preferable to the single-frequency one. Moreover, when noise is present in the measurements, increasing the length of integration interval can be a remedy for effects of noise on estimation accuracy. Observations made on numerical study also indicate that estimation results obtained from a band-limited white-noise input are more accurate than those obtained from the periodic one. Such excitations are adopted in the experimental study in which an electrical system is investigated. The experimental results further confirm the validity and reliability of the proposed method.

1. Introduction

Friction parameter estimation is based on the analysis of measured input and output responses. Our interest is in identifying parameters of basic friction models by making use of vibration properties. For single-dof case, free vibration decrements have been exploited long ago for systems with linear stiffness elements and "small" damping. Free vibration decrements are not applicable if the damping is strong enough to preempt sufficient oscillations. As such, a scheme for extracting Coulomb and viscous friction parameters from forced oscillations based on the analytical solutions of Den Hartog [1] and Hundal [2] for the non-sticking response to harmonic excitations was formulated in Ref. [3]. The limitations of this analytical forced-resonance method are that it is not applicable for damping which is not "small," it relies on analytical solutions of single-dof linear systems, and it does not treat friction models other than Coulomb plus viscous (see for example, Refs. [4–9]).

Thus, an energy balance was proposed as an alternative to identifying friction parameters by using analytical solutions [10]. The energy-dissipation method proposed in Ref. [10] balances the energy input as registered in the force–displacement relationship of the real system against the energy lost of a damping model, with unknown parameters, to develop the identification algorithms. Numerical and experimental

*Tel.: +886 2 2908 9899x4516; fax: +886 2 2906 3269.
E-mail address: liangj@mail.mit.edu.tw

0022-460X/$ - see front matter © 2007 Elsevier Ltd. All rights reserved.
doi:10.1016/j.jsv.2007.07.013

investigations performed in Ref. [10] have shown the reliability and effectiveness of the method. In contrast with Ref. [10], which focused on the single-dof systems, the current study extends the energy-dissipation idea to cope with the multiple dof problems.

Many identification techniques require measured input and output. The energy-dissipation method proposed here falls in that class. Hence, the method can only work in cases where both input and output are measurable. Among the existing techniques, a direct method was proposed by Mohammad et al. [11], where physical parameters, i.e. mass, stiffness and damping, of linear and nonlinear structures can be estimated using measured time data and the least-squares criterion. The method is simple and reliable provided the system is excited in the range where there are modal frequencies. Chen and Tomlinson [12] proposed estimating damping parameters in nonlinear oscillators by utilizing the acceleration, velocity and displacement output and formulating the output in terms of series of frequency response functions. On the other hand, a wavelet-based approach for identifying parameters from nonlinear systems has been proposed by Ghanem and Romeo [13]. The method relies on a wavelet-based discretization of the nonlinear differential equation of motion where orthogonal Daubechies scaling functions are used to track fast variations of the state of the dynamical system. The method might be sensitive to noisy data because responses were projected onto orthogonal space in order to find the wavelet-Galerkin solution of the differential equation. By using orthogonal expansion, details of signal are zoomed so that proper representations of the signal can be formed in terms of expansion coefficients. As such, high-frequency noise might distort expansion coefficients, which in turn could lead to incorrect estimates. The energy-dissipation method is more robust when random noise problem is facing, because such noise can be filtered out through the application of numerical integration.

Unlike the orthogonal expansion methods, the energy-dissipation approach projects the differential equation of motion onto energy spaces. The equations of motion are integrated over time to balance input, kinetic, elastic and dissipated energy involved in the multi-dof vibration system. System parameters are extracted from these energy-balance equations. In addition, different from the direct method proposed by Mohammad et al. in which matrices of large dimensions are involved while singular value decomposition method together with a significance test are required to determine the best set of parameters, our method works in a simpler way because only numerical integrations of system states are necessary to form the identification equations. Similar to the method proposed by Mohammad et al. the energy-dissipation method is not excitation-dependent considering that both periodic and non-periodic excitations can be applied in the approach. It even works for the input-free situations provided the initial conditions are large enough to obtain sufficiently rich responses. When the characteristics of the system are of concern, the energy-dissipation method can be applied to identify nonlinear stiffness or friction model other than Coulomb and viscous, such as the quadratic damping law.

2. Theoretical basis

The energy-dissipation method involves the balance between the energy dissipated by the friction force of a real system against the energy input to the system. This balance results in the "equivalent viscous and Coulomb friction" parameters. The concept is similar to the traditional "equivalent viscous damping" concept seen in undergraduate textbook such as Ref. [14]. To explain the idea, consider a single-dof damped-forced oscillator with the following equation of motion:

$$m\ddot{x} + kx + F(x, \dot{x}) = a(t), \tag{1}$$

where m is the mass, k represents the stiffness, x is the displacement, dots indicate derivatives with respect to time, and $a(t)$ represents the excitation. In addition, $F(x, \dot{x})$ denotes the damping force occurring at the contact interfaces. The energy-dissipation method requires the damping model, used for describing the behaviors of $F(x, \dot{x})$, to have a form of $\alpha F_1(x, \dot{x})$ where α represents the damping coefficient. Although such a requirement imparts limitation on the proposed method, many existing damping models still fall in that category. These include two of the most common friction sources, namely the Coulomb and viscous damping. Other nonlinear damping model satisfying such requirement includes the quadratic damping law.

Multiplying Eq. (1) by dx and integrating the resultant equation along the motion path C yields the following equation:

$$\int_C \{m\ddot{x} + kx + F(x,\dot{x})\}\,dx = \int_C a(t)\,dx.$$

To assist the implementation of integration, the integration variable can be changed to time. Hence

$$\int_T^{t+T_1} \{m\ddot{x} + kx + F(x,\dot{x})\}\dot{x}\,dt = \int_t^{t+T_1} a(t)\dot{x}\,dt,$$

where T_1 denotes a finite time interval. Now, if the following expressions are defined

$$W_d = \int_t^{t+T_1} F(x,\dot{x})\dot{x}\,dt, \quad W_a = \int_t^{t+T_1} a(t)\dot{x}\,dt, \quad W_e = \int_t^{t+T_1} \{m\ddot{x} + kx\}\dot{x}\,dt.$$

Eq. (1) becomes

$$W_d = W_a - W_e. \tag{2}$$

Eq. (2) implies a balance among the dissipated, applied energy and the sum of kinetic and elastic energy. To implement the damping identification, we assume that $x(t)$ (and its derivatives) and $a(t)$ can be measured. Then, the terms involved in Eq. (2) are quantified while $F(x,\dot{x})$ is expressed using an assumed friction model with unknown parameters. By integrating and balancing Eq. (2), one acquires identification equations for the equivalent damping parameters.

When $a(t)$ and $x(t)$ are periodic, one can integrate Eq. (2) over a full cycle of periodic motion. In that case, the contribution of the conservative components of the oscillator $m\ddot{x} + kx$ is zero, so that the following energy-dissipation equation can be obtained:

$$W_d = \int_t^{t+T} F(x,\dot{x})\dot{x}\,dt = \int_t^{t+T} a(t)\dot{x}\,dt = W_a, \tag{3}$$

where T represents the fundamental period of the input and response. To further illustrate the idea, $F(x,\dot{x})$ can be modeled by "viscous plus Coulomb friction" while a harmonic base excitation is adopted for $a(t)$. Therefore, $a(t) = kY_o \cos \omega t$, and

$$W_d = \int_t^{t+T} \{c^*\dot{x} + F_k^* \mathrm{sgn}(\dot{x})\}\dot{x}\,dt = \int_t^{t+T} \{kY_0 \cos \omega t\}\dot{x}\,dt = W_a, \tag{4}$$

where c^* and F_k^* are the equivalent damping parameters to be identified. Here, the Coulomb and viscous damping are chosen out of many other possible candidates. These two damping models may be elementary; but they are also too frequently observed in the real modeling situations (see for instance, Refs. [4–6]) to be ignored. For other more complicated damping models satisfying the form required for the method, i.e. $\alpha F_1(x,\dot{x})$, adjustments can be made to the proposed identification algorithms according to the principles presented. In other words, different nonlinear functions can be adopted to derive proper identification equations.

Eq. (4) can be used to estimate c^* and F_k^* using two excitation levels. Alternatively, more excitation levels can be applied to gain multiple versions of Eq. (4). In the latter case, the number of equations is more than the number of unknown parameters, thus, the least-squares criterion can be applied to improve the robustness of the method. The algorithms outlined above are suitable for estimating parameters from the single-dof vibration system.

The basic concepts and procedures used in the single-dof case can be extended to handle multiple dof problems. To show how the extension can be accomplished, the following equation of motion of a multi-dof system is considered:

$$\mathbf{M}\ddot{\mathbf{x}} + \mathbf{k}\mathbf{x} + \mathbf{c}\dot{\mathbf{x}} + \mathbf{D}(\dot{\mathbf{x}})\mathbf{F_k} = \mathbf{a}(\mathbf{t}),$$

where $\mathbf{M} \in R^{n\times n}$ represents the diagonal mass matrix, n is the number of degrees of freedom, $\mathbf{k} \in R^{n\times n}$ indicates the symmetric stiffness matrix, $\mathbf{c} \in R^{n\times n}$ is the viscous-damping matrix, and $\mathbf{a(t)} \in R^n$ is the input vector.

Moreover, $\mathbf{F_k} \in R^n$ represents a "vector" consisting of Coulomb elements F_{k_i} such that $\mathbf{D}(\dot{\mathbf{x}})\mathbf{F_k}$ models the Coulomb damping occurring at certain locations of the discrete model of the system. To that end, $\mathbf{D}(\dot{\mathbf{x}}) \in R^{n\times n}$ is a matrix comprising of sign functions of relative velocities occurring at contact interfaces. Since, in general, not every damping components appearing in $\mathbf{c}$ and $\mathbf{F_k}$ are unknown quantities, Eq. (4) can be reorganized as

$$\mathbf{M}\ddot{\mathbf{x}} + \mathbf{k}\mathbf{x} + \mathbf{E}(\mathbf{x}, \dot{\mathbf{x}}) + \mathbf{B}(\dot{\mathbf{x}})\mathbf{c}^* + \mathbf{G}(\dot{\mathbf{x}})\mathbf{F}_\mathbf{k}^* = \mathbf{a}(\mathbf{t}) \tag{5}$$

in which $\mathbf{E}(\mathbf{x}, \dot{\mathbf{x}}) \in R^n$ denotes the vector comprising all the "known" damping components multiplied by their associated state functions. On the other hand, $\mathbf{c}^* = [c_1^*, c_2^*, \ldots, c_Q^*]^{\mathrm{T}}$ and $\mathbf{F}_\mathbf{k}^* = [F_{k_1}^*, F_{k_2}^*, \ldots, F_{k_S}^*]^{\mathrm{T}}$ are vectors which contain the "un-identified" viscous and Coulomb-friction parameters. $\mathbf{B}(\dot{\mathbf{x}}) \in R^{n\times Q}$ and $\mathbf{G}(\dot{\mathbf{x}}) \in R^{n\times S}$ denote state-function matrices, which when multiplied separately by $\mathbf{c}^*$ and $\mathbf{F}_\mathbf{k}^*$, can be used to model the viscous and Coulomb damping of the system. In addition, S, $Q \leqslant n$ represent the number of the unknown Coulomb and viscous components.

To formulate the damping-estimation algorithms, $a(t)$ and $x(t)$ are both assumed to be periodic with a common fundamental period, T. Follow the procedures applied in the single-dof system, Eq. (5) is pre-multiplied with $\dot{\mathbf{x}}_i^{\mathrm{T}}$, where $\dot{\mathbf{x}}_i = [0 \ldots \dot{\mathbf{x}}_i \ldots 0]_{n\times 1}^{\mathrm{T}}$, the resultant equation is then integrated over a full cycle of periodic motion. This yields

$$\begin{aligned}&\int_t^{t+T} \dot{\mathbf{x}}_i^{\mathrm{T}}\mathbf{M}\ddot{\mathbf{x}}\,\mathrm{d}t + \int_t^{t+T} \dot{\mathbf{x}}_i^{\mathrm{T}}\mathbf{k}\mathbf{x}\,\mathrm{d}t + \int_t^{t+T} \dot{\mathbf{x}}_i^{\mathrm{T}}\mathbf{E}(\mathbf{x}, \dot{\mathbf{x}})\,\mathrm{d}t + \int_t^{t+T} \dot{\mathbf{x}}_i^{\mathrm{T}}\mathbf{B}(\dot{\mathbf{x}})\mathbf{c}^*\,\mathrm{d}t \\ &\quad + \int_t^{t+T} \dot{\mathbf{x}}_i^{\mathrm{T}}\mathbf{G}(\dot{\mathbf{x}})\mathbf{F}_\mathbf{k}^*\,\mathrm{d}t = \int_t^{t+T} \dot{\mathbf{x}}_i^{\mathrm{T}}\mathbf{a}(\mathbf{t})\,\mathrm{d}t.\end{aligned} \tag{6}$$

Since $\mathbf{M}$ is a diagonal matrix and $\dot{\mathbf{x}}_i$ possesses only one non-zero element, the following equation can be obtained:

$$\begin{aligned}&\int_t^{t+T} \dot{x}_i m_i \ddot{x}_i\,\mathrm{d}t + \int_t^{t+T} \left(\sum_{j=1}^{n} k_{ij}x_j\right)\dot{x}_i\,\mathrm{d}t + \int_t^{t+T} e_i(\mathbf{x}, \dot{\mathbf{x}})\dot{x}_i\,\mathrm{d}t + \int_t^{t+T} \left(\sum_{j=1}^{Q} b_{ij}(\dot{\mathbf{x}})c_j^*\right)\dot{x}_i\,\mathrm{d}t \\ &\quad + \int_t^{t+T} \left(\sum_{j=1}^{S} g_{ij}(\dot{\mathbf{x}})F_{k_j}^*\right)\dot{x}_i\,\mathrm{d}t = \int_t^{t+T} a_i(t)\dot{x}_i\,\mathrm{d}t,\end{aligned} \tag{7}$$

where m_i represents the "ith" diagonal element of $\mathbf{M}$. $\{k_{ij}, j = 1, \ldots, n\}$, $\{b_{ij}, j = 1, \ldots, Q\}$ and $\{g_{ij}, j = 1, \ldots, S\}$ individually denote the "ith" row vector of matrices $\mathbf{k}$, $\mathbf{B}$, and $\mathbf{G}$, whereas a_i and e_i are the "ith" element of vectors $\mathbf{a}(\mathbf{t})$ and $\mathbf{E}(\mathbf{x}, \dot{\mathbf{x}})$.

Since the integration of conservative components over a cycle of periodic motion are zeros, one has $\int_t^{t+T} \dot{x}_i m_i \ddot{x}_i\,\mathrm{d}t = 0$ and $\int_t^{t+T} k_{ii}x_i\dot{x}_i\,\mathrm{d}t = 0$. Eq. (7) can then be recast into

$$\begin{aligned}&\int_t^{t+T} \left(\sum_{j=1}^{Q} b_{ij}(\dot{\mathbf{x}})c_j^*\right)\dot{x}_i\,\mathrm{d}t + \int_t^{t+T} \left(\sum_{j=1}^{S} g_{ij}(\dot{\mathbf{x}})F_{k_j}^*\right)\dot{x}_i\,\mathrm{d}t \\ &\quad = \int_t^{t+T} a_i(t)\dot{x}_i\,\mathrm{d}t - \int_t^{t+T} \left(\sum_{\substack{j=1 \\ j\neq i}}^{n} k_{ij}x_j\right)\dot{x}_i\,\mathrm{d}t - \int_t^{t+T} e_i\dot{x}_i\,\mathrm{d}t\end{aligned}$$

or equivalently,

$$\begin{aligned}&c_1^*\int_t^{t+T} b_{i1}\dot{x}_i\,\mathrm{d}t + c_2^*\int_t^{t+T} b_{i2}\dot{x}_i\,\mathrm{d}t + \cdots + c_Q^*\int_t^{t+T} b_{iQ}\dot{x}_i\,\mathrm{d}t + F_{k_1}^*\int_t^{t+T} g_{i1}\dot{x}_i\,\mathrm{d}t \\ &\quad + F_{k_2}^*\int_t^{t+T} g_{i2}\dot{x}_i\,\mathrm{d}t + \cdots + F_{k_S}^*\int_t^{t+T} g_{iS}\dot{x}_i\,\mathrm{d}t \\ &\quad = \int_t^{t+T} a_i(t)\dot{x}_i\,\mathrm{d}t - \int_t^{t+T} \left(\sum_{\substack{j=1 \\ j\neq i}}^{n} k_{ij}x_j\right)\dot{x}_i\,\mathrm{d}t - \int_t^{t+T} e_i\dot{x}_i\,\mathrm{d}t.\end{aligned} \tag{8}$$

The procedures described above can be repeated for every single-dof of the system. Thus, n equations similar to Eq. (8) are resulted which can be expressed as the followings:

$$c_1^*\tau_{i1} + c_2^*\tau_{i2} + \cdots + c_Q^*\tau_{iQ} + F_{k_1}^*\gamma_{i1} + F_{k_2}^*\gamma_{i2} \cdots + F_{k_S}^*\gamma_{iS} = \beta_i, \quad i = 1, 2, \ldots, n, \tag{9}$$

where

$$\tau_{ij} = \int_t^{t+T} b_{ij}(\dot{\mathbf{x}})\dot{x}_i \, \mathrm{d}t, \quad i = 1, 2, \ldots, n, \quad j = 1, 2, \ldots, Q, \tag{10}$$

$$\gamma_{ij} = \int_t^{t+T} g_{ij}(\dot{\mathbf{x}})\dot{x}_i \, \mathrm{d}t, \quad i = 1, 2, \ldots, n, \quad j = 1, 2, \ldots, S, \tag{11}$$

$$\beta_i = \int_t^{t+T} a_i(t)\dot{x}_i \, \mathrm{d}t - \int_t^{t+T} \left(\sum_{\substack{j=1 \\ j \neq i}}^{n} k_{ij}x_j \right) \dot{x}_i \, \mathrm{d}t - \int_t^{t+T} e_i(\dot{\mathbf{x}})\dot{x}_i \, \mathrm{d}t, \quad i = 1, 2, \ldots, n. \tag{12}$$

It is worth to emphasize that Eq. (9) is the crux of the identification algorithms. The left-hand side of this equation collects all the dissipation energy that involves the un-identified damping coefficients. In contrast, the right-hand side of Eq. (9) consists of the "known" information obtained from the input, elastic, kinetic and dissipated energy involving some "known" damping coefficients. Thus, unknown damping coefficients, $\mathbf{c}^*, \mathbf{F}_\mathbf{k}^*$, can be extracted using the measured input and output of the system.

Eq. (9) can also be organized in a matrix form, yielding

$$A\,\underline{P} = \underline{U}, \tag{13}$$

where A is a matrix for which each row is composed of known quantities τ_{ij} or γ_{ij}. On the other hand, $\underline{P}$ indicates a column vector consists of the unknown damping parameters. Finally, $\underline{U}$ is a column vector carrying the known information obtained from the input, elastic and kinetic energy of the system. In many circumstances, especially the experimental ones, the least-squares criterion can be applied to improve the robustness of the identification method. To do so, more excitations are adopted to generate more identification equations than the number of unknown parameters. Then, the optimal solution for vector $\underline{P}$, in the least-squares sense, becomes

$$\underline{P} = (A^{\mathrm{T}}A)^{-1}A^{\mathrm{T}}\,\underline{U}. \tag{14}$$

Eq. (14) provides an optimal estimate of the unknown parameters, along with a residual $\underline{r} = A\,\underline{P} - \underline{U}$ which is generally non-zero. The residual can serve as an indicator of the quality of the damping model. In this study, it tells whether "viscous plus Coulomb" model can adequately describe friction behaviors occurring at different contact interfaces. Details of implementing the energy-dissipation identification method augmented with the least-squares criterion will be elaborated in the numerical and experimental verifications.

It should also be emphasized that the algorithms presented in Eqs. (9)–(12) are only suitable for the case where both input and response are periodic data. When $a(t)$ is non-periodic, the interval of integration can be of arbitrary length, whereas the contributions of conservative terms do not vanish after integration. As a result, the expression of Eq. (12) changes to

$$\beta_i = \int_t^{t+T} a_i(t)\dot{x}_i \, \mathrm{d}t - \int_t^{t+T} m_i\ddot{x}_i\dot{x}_i \, \mathrm{d}t - \int_t^{t+T} \left(\sum_{j=1}^{n} k_{ij}x_j \right) \dot{x}_i \, \mathrm{d}t - \int_t^{t+T} e_i(\dot{\mathbf{x}})\dot{x}_i \, \mathrm{d}t, \quad i = 1, 2, \ldots, n. \tag{12a}$$

Here, the integrating interval, T, is an arbitrary time interval rather than the fundamental period of $a(t)$ and $x(t)$. Eqs. (9)–(11) and (12a) can be adopted to estimate damping parameters in a general-input problem.

Furthermore, in order to measure "the goodness of fit" between the estimated system response (the response obtained from numerical simulation using the identified damping coefficients) and the simulated or experimental one, a normalized mean square error (MSE) of "acceleration" (used in the numerical studies) or "velocity" (used in the experimental case) signal is adopted. The same indicator was also chosen in Ref. [11].

Taking acceleration signal as an example, the MSE percentage can be defined as

$$\mathrm{MSE}_i = \left[\frac{\{\sum_{j=1}^{N_p}(\ddot{x}_{ij} - \tilde{\ddot{x}}_{ij})^2\}}{N_p\sigma^2_{\ddot{x}_i}}\right] \times 100, \quad i = 1, 2, \ldots, n, \tag{15}$$

where $\ddot{x}$ is the simulated or measured acceleration, while $\tilde{\ddot{x}}$ is the estimated one. Meanwhile, N_p is the number of data points, and $\sigma^2_{\ddot{x}}$ indicates the variance of the simulated or measured acceleration.

3. Application of the method to simulation data

A numerical system with known parameter values is selected to validate the proposed schemes. Both the periodic- and general-input cases are considered. In implementing the method, the differential equations of motion are first formulated in a matrix form similar to Eq. (5). Then, a stiff, low-order ordinary differential equation (ODE) solver of Bogacki and Shampire (ode23tb) is adopted to integrate the ODEs of the numerical systems at a constant sampling rate, after converting the ODEs to first-order form [15]. Depending on the type of excitation, Simpson's rule is adopted to obtain τ_{ij}, γ_{ij}, and β_i in accordance with the contexts shown in Eqs. (10)–(12) or (10), (11) and (12a). Then, in order to examine the method's sensitivity to noisy measurement, white random noise is added to the simulated data. The equivalent damping estimates obtained from the noise-contaminated data are compared to those obtained from the noise-free case.

Fig. 1 shows the schematic of the 3-dof vibration system to be numerically studied. The same system has been studied in Ref. [11]. According to Fig. 1, the following equations of motion can be obtained:

$$\begin{bmatrix} m_1 & 0 & 0 \\ 0 & m_2 & 0 \\ 0 & 0 & m_3 \end{bmatrix} \begin{Bmatrix} \ddot{x}_1 \\ \ddot{x}_2 \\ \ddot{x}_3 \end{Bmatrix} + \begin{bmatrix} (c^*_{11} + c^*_{12}) & -c^*_{12} & 0 \\ -c^*_{12} & (c^*_{12} + c^*_{23}) & -c^*_{23} \\ 0 & -c^*_{23} & (c^*_{23} + c^*_{33}) \end{bmatrix} \begin{Bmatrix} \dot{x}_1 \\ \dot{x}_2 \\ \dot{x}_3 \end{Bmatrix}$$

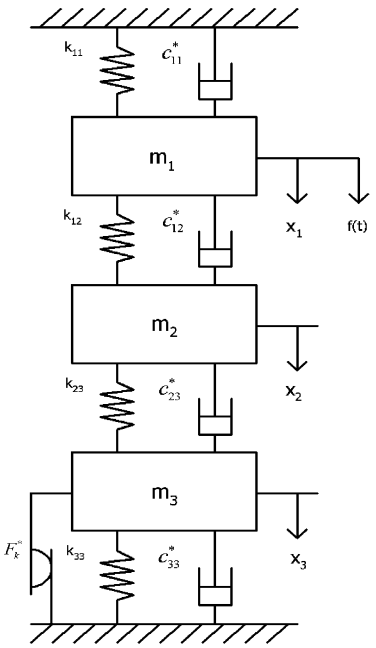

Fig. 1. Three-dof system with friction link between mass 3 and ground.

$$+\begin{bmatrix}(k_{11}+k_{12}) & -k_{12} & 0\\ -k_{12} & (k_{12}+k_{23}) & -k_{23}\\ 0 & -k_{23} & (k_{23}+k_{33})\end{bmatrix}\begin{Bmatrix}x_1\\ x_2\\ x_3\end{Bmatrix}+\begin{Bmatrix}0\\ 0\\ \mathrm{sgn}(\dot{x}_3)\end{Bmatrix}F_k^*=\begin{Bmatrix}f(t)\\ 0\\ 0\end{Bmatrix}. \tag{16}$$

It can be seen in Eq. (16) that there are four viscous-damping parameters, namely c_{11}^*, c_{12}^*, c_{23}^* and c_{33}^*, and one Coulomb parameter, F_k^*, to be estimated. From the context of Eq. (5), Eq. (16) can be converted into

$$\begin{bmatrix}m_1 & 0 & 0\\ 0 & m_2 & 0\\ 0 & 0 & m_3\end{bmatrix}\begin{Bmatrix}\ddot{x}_1\\ \ddot{x}_2\\ \ddot{x}_3\end{Bmatrix}+\begin{bmatrix}(k_{11}+k_{12}) & -k_{12} & 0\\ -k_{12} & (k_{12}+k_{23}) & -k_{23}\\ 0 & -k_{23} & (k_{23}+k_{33})\end{bmatrix}\begin{Bmatrix}x_1\\ x_2\\ x_3\end{Bmatrix}$$
$$+\begin{bmatrix}\dot{x}_1 & \dot{x}_1-\dot{x}_2 & 0 & 0\\ 0 & \dot{x}_2-\dot{x}_1 & \dot{x}_2-\dot{x}_3 & 0\\ 0 & 0 & \dot{x}_3-\dot{x}_2 & \dot{x}_3\end{bmatrix}\begin{Bmatrix}c_{11}^*\\ c_{12}^*\\ c_{23}^*\\ c_{33}^*\end{Bmatrix}+\begin{Bmatrix}0\\ 0\\ \mathrm{sgn}(\dot{x}_3)\end{Bmatrix}F_k^*=\begin{Bmatrix}F_0\cos\omega t\\ 0\\ 0\end{Bmatrix}. \tag{17}$$

According to Eq. (17), a periodic excitation, $f(t)=F_0\cos\omega t$, is assumed to excite the system at coordinate 1. Thus, the identification equations can be determined using Eq. (17) and the contexts of Eqs. (9)–(12), yielding

$$\tau_{11}c_{11}^*+\tau_{12}c_{12}^*=\beta_1, \tag{18}$$

$$\tau_{22}c_{12}^*+\tau_{23}c_{23}^*=\beta_2, \tag{19}$$

$$\tau_{33}c_{23}^*+\tau_{34}c_{33}^*+\gamma_{31}F_k^*=\beta_3, \tag{20}$$

where

$$\tau_{11}=\int_t^{t+T}\dot{x}_1^2\,\mathrm{d}t,\quad \tau_{12}=\int_t^{t+T}\dot{x}_1(\dot{x}_1-\dot{x}_2)\,\mathrm{d}t,\quad \beta_1=\int_t^{t+T}\dot{x}_1(F_o\cos\omega t+k_{12}x_2)\,\mathrm{d}t, \tag{21}$$

$$\tau_{22}=\int_t^{t+T}\dot{x}_2(\dot{x}_2-\dot{x}_1)\,\mathrm{d}t,\quad \tau_{23}=\int_t^{t+T}\dot{x}_2(\dot{x}_2-\dot{x}_3)\,\mathrm{d}t,\quad \beta_2=\int_t^{t+T}\dot{x}_2(k_{12}x_1+k_{23}x_3)\,\mathrm{d}t, \tag{22}$$

$$\tau_{33}=\int_t^{t+T}\dot{x}_3(\dot{x}_3-\dot{x}_2)\,\mathrm{d}t,\quad \tau_{34}=\int_t^{t+T}\dot{x}_3^2\,\mathrm{d}t,\quad \gamma_{31}=\int_t^{t+T}\dot{x}_3\mathrm{sgn}(\dot{x}_3)\,\mathrm{d}t,\quad \beta_3=\int_t^{t+T}\dot{x}_3(k_{23}x_2)\,\mathrm{d}t. \tag{23}$$

Note that when the general input is considered, all β_i, $i=1,2,3$ presented above should be changed based on the contexts of Eq. (12a). Note that each of the differential equations appearing in Eq. (16) is of second order. Theoretically, each of these equations can be used to solve for two unknown parameters provided persistent excitation conditions are satisfied [16]. Hence, the maximal number of unknowns that can be estimated in this example is six. Here, the system has only five unknowns. As such, one can choose to excite the system with two different amplitudes, while all three differential equations of (16) are adopted. Alternatively, one can choose to use all three ODEs of Eq. (16) with more than two excitation levels, so that excessively more algebraic equations than the number of unknowns are obtained. In that case, more robust estimations can be gained through the application of the least-squares criterion. Based on the contexts of Eq. (13) and

Eqs. (18)–(23), one ends up with $A\,\underline{P} = \underline{U}$, where

$$A = \begin{bmatrix} \tau_{11}^1 & \tau_{12}^1 & 0 & 0 & 0 \\ 0 & \tau_{22}^1 & \tau_{23}^1 & 0 & 0 \\ 0 & 0 & \tau_{33}^1 & \tau_{34}^1 & \gamma_{31}^1 \\ \vdots & \vdots & \vdots & \vdots & \vdots \\ \tau_{11}^k & \tau_{12}^k & 0 & 0 & 0 \\ 0 & \tau_{22}^k & \tau_{23}^k & 0 & 0 \\ 0 & 0 & \tau_{33}^k & \tau_{34}^k & \gamma_{31}^k \\ \vdots & \vdots & \vdots & \vdots & \vdots \\ \tau_{11}^l & \tau_{12}^l & 0 & 0 & 0 \\ 0 & \tau_{22}^l & \tau_{23}^l & 0 & 0 \\ 0 & 0 & \tau_{33}^l & \tau_{34}^l & \gamma_{12}^l \end{bmatrix}_{3l\times 5}, \quad \underline{P} = \begin{bmatrix} c_{11}^* \\ c_{12}^* \\ c_{23}^* \\ c_{33}^* \\ F_k^* \end{bmatrix}, \quad \underline{U} = \begin{bmatrix} \beta_1^1 \\ \beta_2^1 \\ \beta_3^l \\ \vdots \\ \beta_1^k \\ \beta_2^k \\ \beta_3^k \\ \vdots \\ \beta_1^l \\ \beta_2^l \\ \beta_3^l \end{bmatrix}_{3l\times 1}.$$

Here, the superscript "k" denotes an arbitrary excitation level, whereas "l" indicates the total number of excitation levels applied. The optimal solution based on the least-squares criterion can be written as $\underline{P} = (A^{\mathrm{T}}A)^{-1}A^{\mathrm{T}}\,\underline{U}$. This approach will be adopted in the numerical and experimental investigations described in the following sections.

3.1. Numerical study of the 3-dof system: the periodic-excitation case

Numerical simulations are performed with respect to the system shown in Fig. 1 using the following parameters: $m_1 = 1.5\,\mathrm{kg}$, $m_2 = 1.3\,\mathrm{kg}$, $m_3 = 2.0\,\mathrm{kg}$, $k_{11} = k_{12} = k_{23} = k_{33} = 1\times 10^4\,\mathrm{N/m}$, $c_{11}^* = c_{12}^* = c_{23}^* = c_{33}^* = 20\,\mathrm{N\,s/m}$, and $F_k^* = 1.0\,\mathrm{N}$. In periodic validation, four cases are studied which correspond to different excitation and data-processing conditions, as elaborated in Table 1. In Case 1, two sinusoidal inputs of different frequencies ($\omega = 2\pi\times 5$ and $2\pi\times 10$) and amplitudes ($F_0 = 80$ and 200) are adopted. Case 1 is also denoted as the noise-free, mixed-frequency harmonic excitation case. In contrast, in Case 2 (also denoted as the noise-free, single-frequency harmonic excitation case) two single-frequency ($\omega = 2\pi\times 10$) sinusoidals of different amplitudes, $F_0 = 80$ and 200, are selected. Next, the mixed-frequency excitations are adopted again in Case 3. However, this time the system's input and responses are superimposed by a white random noise of 5% of their individual root-mean-squares values. The integration interval, T, used in Cases 1–3 are all equal to 0.2 s which is the fundamental period of 5 and 10 Hz periodical signals. Then, in order to understand whether the length of the integration interval will affect the estimation accuracy, the integration interval, T, is increased from 0.2 to 2 s in Case 4. Case 4 is not only characterized by the much longer integration interval, its data are also contaminated in the same way as that in Case 3.

Table 1
The excitation and noise conditions of the sinusoidal-input cases

	Excitation and noise conditions
Case 1	The mixed-frequency input, excitation 1: $F_o = 80$, $\omega = 2\pi\times 5$; excitation 2: $F_o = 200$, $\omega = 2\pi\times 10$; noise-free data were integrated over 0.2 s
Case 2	The single-frequency input, excitation 1: $F_o = 80$, $\omega = 2\pi\times 10$; excitation 2: $F_o = 200$, $\omega = 2\pi\times 10$; noise-free data were integrated over 0.2 s
Case 3	The mixed-frequency input, excitation 1: $F_o = 80$, $\omega = 2\pi\times 5$; excitation 2: $F_o = 200$, $\omega = 2\pi\times 10$; data contaminated with 5% noise were integrated over 0.2 s
Case 4	The mixed-frequency input, excitation 1: $F_o = 80$, $\omega = 2\pi\times 5$; excitation 2: $F_o = 200$, $\omega = 2\pi\times 10$; data contaminated with 5% noise were integrated over 2 s

Table 2
The optimal estimates, MSE indicators (all based on $F_o = 100$, $\omega = 2\pi \times 10$) and residuals obtained in simulation Case 1–4

Case 1				Case 2				Case 3				Case 4			
$\tilde{c}_{11}^*$	20.04	MSE_1	0.0012%	$\tilde{c}_{11}^*$	19.26	MSE_1	0.0038%	$\tilde{c}_{11}^*$	19.70	MSE_1	0.029%	$\tilde{c}_{11}^*$	19.60	MSE_1	0.0016%
$\tilde{c}_{12}^*$	20.05	MSE_2	0.0013%	$\tilde{c}_{12}^*$	18.16	MSE_2	0.0014%	$\tilde{c}_{12}^*$	17.25	MSE_2	0.032%	$\tilde{c}_{12}^*$	19.32	MSE_2	0.0023%
$\tilde{c}_{23}^*$	20.19	MSE_3	0.0013%	$\tilde{c}_{23}^*$	23.41	MSE_3	0.0029%	$\tilde{c}_{23}^*$	18.45	MSE_3	0.035%	$\tilde{c}_{23}^*$	20.30	MSE_3	0.0021%
$\tilde{c}_{33}^*$	20.09	r	7.94e−4	$\tilde{c}_{33}^*$	20.80	r	9.49e−5	$\tilde{c}_{33}^*$	20.08	r	3.57e−2	$\tilde{c}_{33}^*$	20.18	r	6.98e−3
$\tilde{F}_k^*$	1.01			$\tilde{F}_k^*$	1.01			$\tilde{F}_k^*$	0.85			$\tilde{F}_k^*$	1.02		

Optimal estimates based on the least-squares criterion are sought in the numerical investigations. According to each set of optimal estimates, $\tilde{c}_{11}^*, \tilde{c}_{12}^*, \tilde{c}_{23}^*, \tilde{c}_{33}^*$ and $\tilde{F}_k^*$, a residual, r, is computed. The value of r indicates whether the Coulomb and viscous model can adequately describe the friction behaviors of the system. In addition, numerical simulations, corresponding to these optimal parameters together with the excitation condition:$F_o = 100$, $\omega = 2\pi \times 10$ are conducted to obtain the "estimated" acceleration responses. These "estimated" responses are then compared to the "simulated" ones obtained using the given parameters. The MSE indicators are computed accordingly. The MSE indicators quantify the closeness between the estimated and simulated acceleration responses.

The damping estimates are listed in Table 2. Obviously, for the noise-free cases, i.e. Cases 1 and 2, the viscous-damping estimates obtained from the mixed-frequency case are better than that of the single-frequency case while the Coulomb ones are the same. Our speculations for the difference between the viscous estimates are that forcing system with more than one frequency (both near the resonant frequencies, which are approximately equal to 13, 14.3 and 16 Hz, respectively) will excite richer responses of the system. Thus, more information regarding the viscous damping is provided in these responses, which in turn lead to better viscous estimations. Other possible explanation includes that using two levels of excitation with the same frequency theoretically will lead to linear relationships between velocities and therefore between the viscous terms of the equations obtained from the two tests. To that end, the resultant equations are less independent than those obtained from the mixed-frequency case. The latter speculation somewhat explains why the Coulomb estimates is not so sensitive (compared to the viscous case) to different excitation conditions. Moreover, because the 3-dof vibration system may have very complicated responses, other mechanism could exist. For instance, our experiences on numerical study show that the phase relationship between the system states appearing in the definite integrals of Eqs. (21)–(23) also accounts. More specifically, if the phase relationship between the system states of the monotonically non-decreasing integrals (which can be found among Eqs. (21)–(23)) results in larger values, more accurate estimates can be obtained.

Next, the MSE values associated with accelerations $\ddot{x}_1, \ddot{x}_2, \ddot{x}_3$ are computed according to the context of Eq. (15) together with the simulated and estimated data. The MSE values of Cases 1 and 2 are very small. This occurs because the MSE value is not only proportional to the errors between the simulated and estimated acceleration but also inversely proportional to the variance of the simulated acceleration data. The former is small while the latter is large in Cases 1 and 2. The residuals associated with these two cases are 7.94e−4 and 9.49e−5, respectively. These values are also very small.

Unlike Cases 1 and 2, the input and response signals of Case 3 are contaminated by random noise. Fig. 2 presents the features of the contaminated data in which $F_0 = 80$ and $\omega = 2\pi \times 5$. Based on the contaminated data, the optimal estimates of Case 3 are obtained and included in Table 2. Because the forcing conditions of Case 3 are the same as those of Case 1, the results obtained in the former should be compared to the latter to find the effects of random noise on estimation accuracy. From these results, one finds that both the viscous and Coulomb estimates deteriorate due to the presence of random noise. In fact, the largest error of viscous estimate increases from 1% to 13.75% while the error of Coulomb estimate increases from 1% to 15%. Next, two simulations corresponding to the given and estimated parameters, respectively, are conducted and presented in Fig. 3. Since no random noise has been added to these acceleration data, substantially cleaner features as compared to Fig. 2 appear in Fig. 3. In addition, relative difference between the estimated and simulated acceleration pairs are also shown in Fig. 3. It can be observed from Fig. 3 that even though the damping estimates

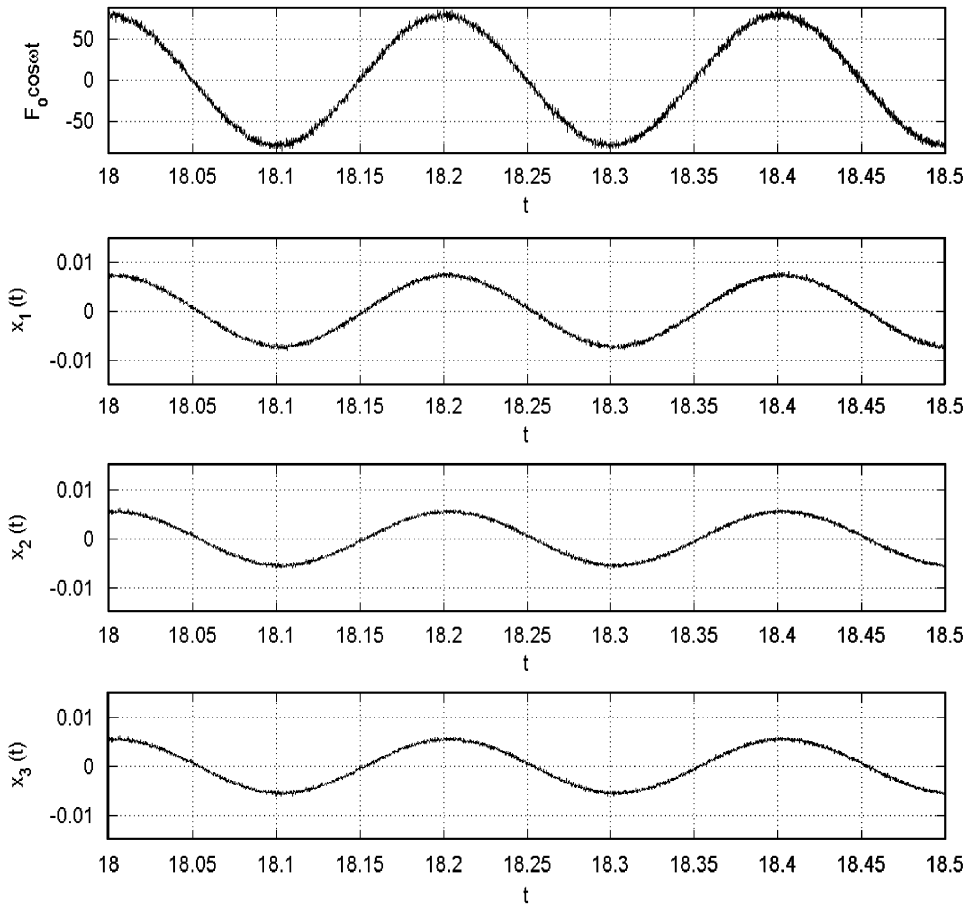

Fig. 2. The noise-contaminated signals obtained by adding a white random noise to the simulated data ($F_o = 80.0$).

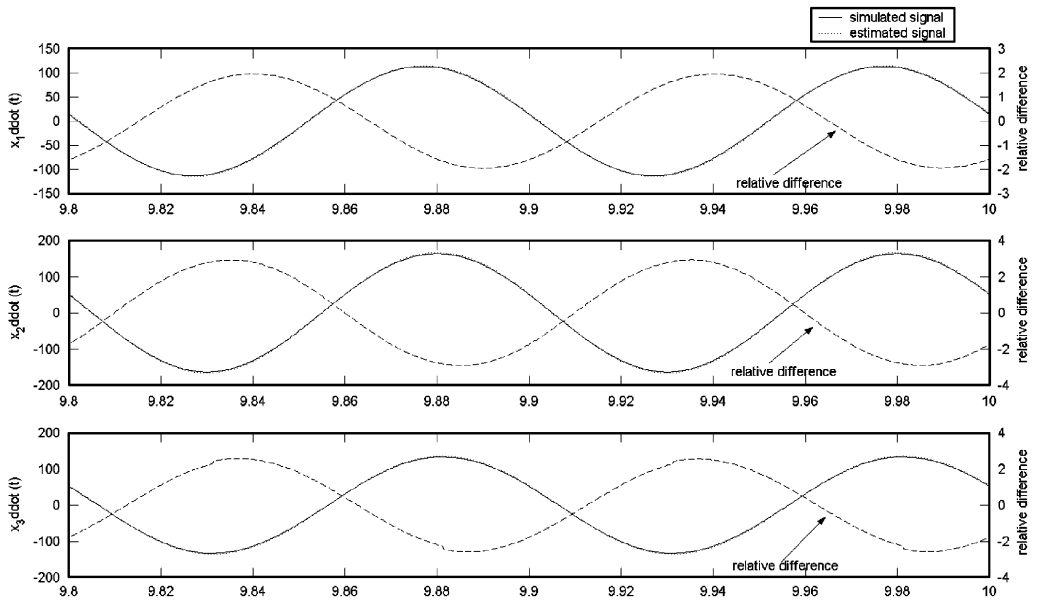

Fig. 3. Comparison between the estimated (dotted line) and the simulated (solid line) acceleration responses of Case 3, the relative difference between the estimated and simulated acceleration are shown in dashed line.

obtained from Case 3 seem to be less accurate, the agreements between the simulated and estimated responses are visually quite acceptable. This can be further confirmed by the small magnitudes of the relative differences. Nonetheless, the MSE values and the residual of Case 3 are evidently worse than those of Cases 1 and 2.

Finally, the length of integration interval is increased from 0.2 to 2 s in Case 4. Because the data in Case 4 are contaminated in the same way as that in Case 3, the identification results of both cases should be compared to each other. Based on the optimal estimates of Cases 3 and 4, one finds that increasing the integration period can dramatically improve the estimation accuracy. The improvements include that for example, the estimation error of F_k^* reduces from 15% to 2% while the largest estimation error of viscous damping reduces from 13.75% to 3.4%. The improvements take place in both viscous and Coulomb estimates, and consequently the MSE indicators and the residual. The results are encouraging, considering that the estimates in Case 3 are not so satisfactory. Our explanation for such an improvement is that increasing the integration interval would also increase the resultant values obtained from some of the monotonically non-decreasing integrals presented in Eqs. (21)–(23). On the other hand, the random noise superimposed in the signal is filtered out through the application of integration. Since the significant information required in extracting damping parameters is accumulated while the effects of noise are filtered out, the improvements of the estimates can be predicted. To summarize, through numerical investigations, one finds that the mixed-frequency sinusoidal excitation provides better estimates than the single-frequency one when the periodic excitations are of concern. Moreover, when noisy data are met, increasing the integration interval can be a remedy for the effects of noise.

3.2. Numerical study of the 3-dof system: non-periodic excitation case

A couple of changes have to be made before the identification of non-periodic data can be performed. These changes include: (1) the energy contribution of the conservative components will be considered and (2) the integration interval can be of arbitrary length instead of a complete forcing period. In performing numerical experiments on the general-input case, the system is assumed to be excited at coordinate 1 with two band-limited (in the frequency range 5–50 Hz) white noise signals with zero mean and of rms levels 10 and 40, respectively. Two cases are investigated in the general-input validations. The first case deals with the noise-free data and is denoted as Case 5, whereas the second case, also denoted as Case 6, deals with the contaminated data. Details of the data-processing and excitation conditions of these cases are listed in Table 3. For comparison reason, the parameter values are kept the same as those in the periodic-input case.

The identification procedures are basically the same as those used in the periodic cases. To this end, the optimal damping estimates Cases 5 and 6 are obtained and presented in Table 4. According to Table 4, one

Table 3
The excitation and noise conditions of the general-input cases

	Excitation and noise conditions
Case 5	Band-limited (5–50 Hz) white noise with zero mean, excitation 1: rms level = 10; excitation 2: rms level = 40; noise-free data were integrated over 2 s
Case 6	Band-limited (5–50 Hz) white noise with zero mean, excitation 1: rms level = 10; excitation 2: rms level = 40; data contaminated with 5% noise were integrated over 2 s

Table 4
The optimal estimates, MSE indicators (based on input with rms level = 40) and residuals obtained in simulation Case 5 and 6

Case 5				Case 6			
$\tilde{c}_{11}^*$	20.0002	MSE_1	0.029%	$\tilde{c}_{11}^*$	19.9986	MSE_1	0.037%
$\tilde{c}_{12}^*$	20.0010	MSE_2	0.047%	$\tilde{c}_{12}^*$	20.0010	MSE_2	0.074%
$\tilde{c}_{23}^*$	19.9990	MSE_3	0.091%	$\tilde{c}_{23}^*$	19.9990	MSE_3	0.107%
$\tilde{c}_{33}^*$	20.0036	r	9.37e−6	$\tilde{c}_{33}^*$	20.0004	r	2.32e−6
$\tilde{F}_k^*$	0.999995			$\tilde{F}_k^*$	0.99995		

can see that the results of Case 5 are extremely accurate. In fact, these estimate are even better than those of Case 1 considering that both cases are associated with perfect models and clean data. The highly accurate estimates obtained for Case 5 may be reasonable because the random input has a relatively broadband spectrum. Richer response can thus be acquired. These responses in turn provide more information from which more accurate damping parameters are extracted. Note that even though the optimal estimates obtained in Case 5 are extremely accurate, the associated MSE values are an order larger than those of Cases 1 and 2. This happens because the variance of the simulated acceleration in this case is about 100 times smaller than that of Cases 1 and 2. The residual associated with Case 5 is approximately as small as those of Cases 1 and 2.

Similar to the periodic case, in Case 6, we add to the simulated input, velocity and displacement responses a white random noise of 5% of their individual root-mean-squares values. The resultant estimates extracted from the contaminated data are also listed in Table 4. It can be seen that not only the damping estimates but also the MSE indicators and the residual of this case are all as accurate as those of Case 5. This indicates that the band-limited random input is almost free from the effects of the added white noise.

Intuitively, it seems that the random-input approach is preferable to the periodic one if only the estimation accuracy is of concern. However, more measurements including acceleration data are required in order to implement the non-periodic identification. This can be a drawback, especially when acceleration data are difficult to obtain. In the next section, experimental validations are conducted on an electrical multi-dof system. The reason for choosing electrical over mechanical system is that the former one is easier to be realized. However, this does not imply that the energy-dissipation method is easier to be implemented in the electrical system too. Because the velocity and acceleration signals are difficult to directly measure in electrical system, digital differentiation is inevitable. The latter is challenging especially when experimental identification task is involved.

4. Experimental validations

It is true that if the tests on a mechanical system, such as the 3-dof system studied in the numerical simulations, are available, they can provide stronger validation of the method. But, on the other hand, if the previous 3-dof data is not available, then it becomes difficult to make this substitution. To this end, the experimental investigations are conducted on a two-loop electrical network consisting of two resistor–inductor–capacitor (RLC) series circuits. The author would like to point out that the electrical circuit applied in the study is not simply another simulation, since their corresponding accuracies are different. As a matter of fact, the resister and capacitor adopted in this study individually have a 5–10% uncertainty of their rated resistance and capacitance values. The reported resistance and capacitance values obtained by careful measurements are also slightly temperature and frequency dependent. Thus, uncertainty of parameters exists in the experimental system.

Fig. 4 shows the schematic diagram of the experimental system where $v(t)$ represents the voltage input while $v_{c1}(t)$ and $v_{c2}(t)$ denote the voltage output corresponding to capacitors C_1 and C_2, respectively. By using mesh or nodal analysis, the differential equations, which relate the voltage input to the voltage output, can be

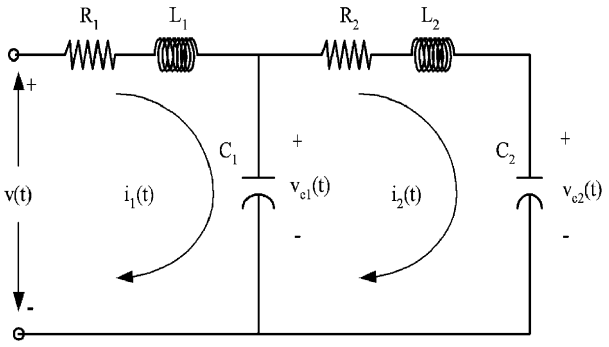

Fig. 4. Schematic diagram of the experimental system.

formulated as

$$L_1C_1\frac{d^2v_{c1}(t)}{dt^2}+R_1C_1\frac{dv_{c1}(t)}{dt}+v_{c1}(t)-\frac{C_2}{C_1}v_{c2}(t)=v(t), \tag{25}$$

$$L_2C_2\frac{d^2v_{c2}(t)}{dt^2}+R_2C_2\frac{dv_{c2}(t)}{dt}+v_{c2}(t)+\frac{C_2}{C_1}v_{c2}(t)-v_{c1}(t)=0, \tag{26}$$

where $R_1(R_2)$, $L_1(L_2)$, and $C_1(C_2)$ denote the resistance, inductance and capacitance of loops 1 and 2. In order to apply the proposed identification algorithms to the electrical system, direct equivalences (which might be different from the traditional ones as seen in Ref. [17]) between the electrical and mechanical systems are adopted. To that end, products L_iC_i and R_iC_i are equivalent to the mass and viscous-damping components of a 2-dof mechanical system, respectively, whereas the output voltage, $v_{c1}(t)$ and $v_{c2}(t)$, are equivalent to the displacement responses of the same mechanical system. In accordance with these direct equivalences, the proposed algorithms presented in Eqs. (9)–(12), or (9)–(11) and (12a) can be adopted to identify the R_iC_i values.

Additionally, according to the numerical studies performed in the previous section, one realizes that in order to gain rich response and hence better estimates from the system, random excitation will be a better choice compared to the mixed-frequency harmonic one. Therefore, band-pass limited white noise excitations are chosen as voltage input to the double RLC circuits, leading to the following identification equations:

$$\tau_{11}\tilde{C}_1^*=\beta_1, \tag{27}$$

$$\tau_{22}\tilde{C}_2^*=\beta_2, \tag{28}$$

where

$$\tau_{11}=\int_t^{t+T}\dot{v}_{c1}^2(t)\,dt,\quad \beta_1=\int_t^{t+T}\left[v(t)-L_1C_1\ddot{v}_{c1}(t)-v_{c1}(t)+\frac{C_2}{C_1}v_{c2}(t)\right]\dot{v}_{c1}(t)\,dt, \tag{29}$$

$$\tau_{22}=\int_t^{t+T}\dot{v}_{c2}^2(t)\,dt,\quad \beta_2=\int_t^{t+T}\left[v_{c1}(t)-L_2C_2\ddot{v}_{c2}(t)-(1+\frac{C_2}{C_1})v_{c2}(t)\right]\dot{v}_{c2}(t)\,dt. \tag{30}$$

Here, the integration interval, T, can be of an arbitrary length. $\tilde{C}_1^*$ and $\tilde{C}_2^*$ denote the estimates of the electrical parameters R_1C_1 and R_2C_2. To avoid confusion, these unidentified parameters will be designated as the "electrical-viscous parameters" and denoted as C_1^* and C_2^* hereafter.

Next, experimental tests are conducted on the double-RLC series circuit in which aluminum electrolytic capacitor, powder-core inductors and carbon resistors are adopted. By careful measurement, the following values are obtained: $R_1=163\,\Omega$, $R_1=162\,\Omega$, $L_1=L_2=0.1\,\mathrm{H}$, $C_1=960\,\mu\mathrm{F}$, $C_2=956\,\mu\mathrm{F}$. Therefore, the reference values of the un-identified "target" parameters are: $R_1C_1=0.157$ and $R_2C_2=0.155$. Note that the resistor and capacitor adopted in this study individually have 5–10% uncertainty of their rated resistance and capacitance values. Moreover, the "measured" resistance and capacitance values shown above are also subjected to temperature and frequency dependence. Therefore, parameter uncertainties do exist in the experimental system.

An arbitrary function generator (Tektronix, TDS3012) is used to excite the electrical system. The function generator is driven by a personal computer through a GPIB-USB interface. A set of random data (generated using the "randn" command of the MATLAB commercial software) is sent to the function generator using the GPIB-USB interface. The random signal is band-pass limited in the frequency range of 1–6 Hz. The low frequency content of the input is intended to excite larger responses from the electrical system. Due to the high damping ratio, the electrical system will not resonate. Therefore, the largest output of the system occurs near DC. Fig. 5 shows features of the typical, post-filtering, voltage input and output of the system.

Because there is noise of small amplitudes superimposed on all of the voltage measurements, a fourth-order low-pass digital filter (elliptic type, realized using MATLAB commercial software) with a cut-off frequency equal to 10 Hz is used. The same filter can also be used to eliminate the 60-Hz power line noise. Additionally, since only voltage outputs, $v_{c1}(t)$ and $v_{c2}(t)$, are measured, other signals such as $\dot{v}_{c1}(t)$, $\dot{v}_{c2}(t)$, $\ddot{v}_{c1}(t)$ and $\ddot{v}_{c2}(t)$ are

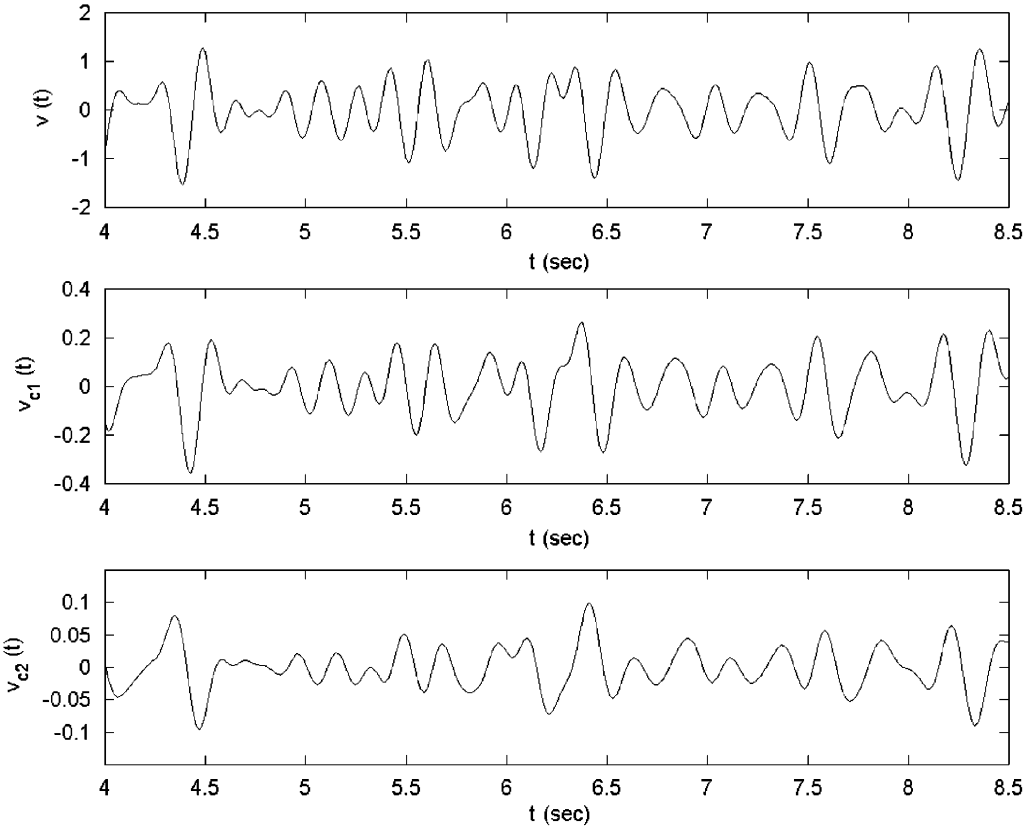

Fig. 5. A typical plot showing the random input and responses of the electrical RLC series circuits.

Table 5
The estimates obtained from voltage measurements of the electrical system

Test	$\tilde{C}_1^*$	$\tilde{C}_2^*$	MSE_1 (%)	MSE_2 (%)
1	0.151	0.147	4.78	1.70
2	0.154	0.147	4.94	1.93
3	0.154	0.146	4.69	1.93
4	0.153	0.151	4.62	2.23
5	0.152	0.140	5.09	1.55

obtained by digital differentiations. Serious fluctuations are introduced by these digital differentiations. Fortunately, the same low-pass filter can also overcome the noise problem introduced by the numerical differentiations. Finally, to avoid the effects of the "phase" distortions caused by the filtering, which may in turn affect the estimation results, all the signals used in the identification process are low-pass filtered using the same filter.

According to the contexts of Eqs. (27) and (28), a single test will be sufficient to gain quick estimates of the electrical-viscous parameters, C_1^* and C_2^*, five tests are indeed adopted. Thus, the least-squares criterion can be applied. Table 5 lists the estimates obtained from the five tests using solely Eqs. (27) and (28). Meanwhile, the least-squares estimates resulted from the same five tests are: $\tilde{C}_{1LS}^* = 0.153$ and $\tilde{C}_{2LS}^* = 0.147$. The associated residual is 0.0110. Compared to the reference values, which are 0.157 and 0.155, respectively, one can see that the proposed method can accurately identify the electrical-viscous parameters. Based on the least-squares estimates the estimation errors are all below 6%. The accuracies are quite acceptable considering the facts that

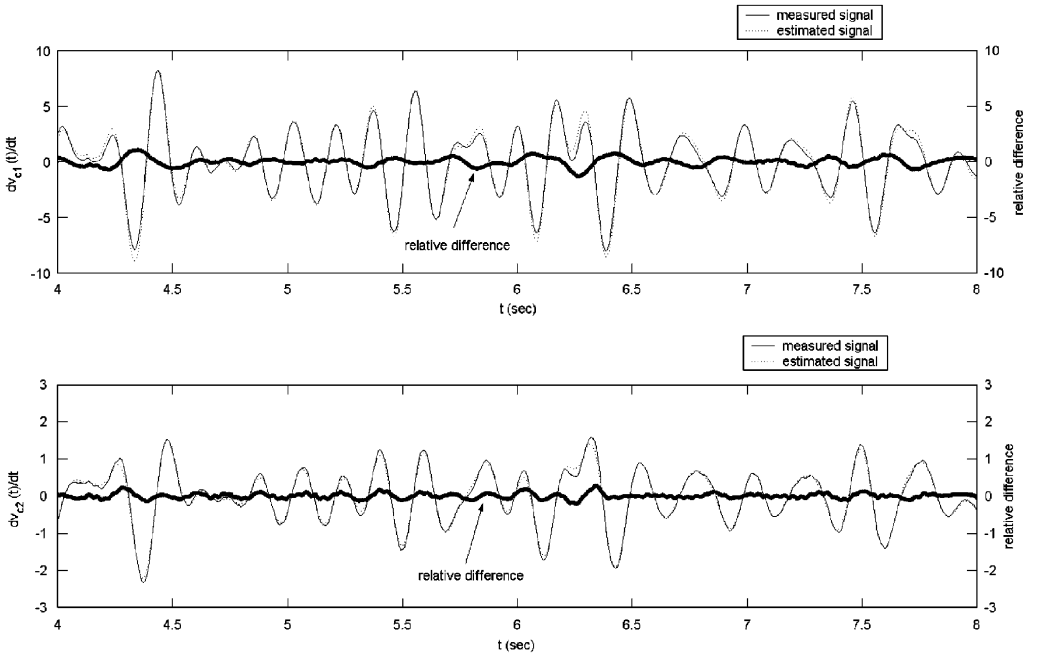

Fig. 6. A comparison plot shows the simulated (dotted line) and measured (solid line) random responses of the experimental system.

digital differentiation and low-pass filtering operations are both involved. These operations can more-or-less affect the identification results although cautions have been taken. Furthermore, the low residual indicates that the viscous-damping model can approximately describe the system behaviors.

Similar to the numerical case, the "estimated" parameters and the band-limited random input are used to simulate the first derivatives of the voltage output, i.e. $\dot{v}_{c1}(t)$ and $\dot{v}_{c2}(t)$. These results are presented in Fig. 6 and denoted as the "estimated" signal. The estimated signal are compared to the "measured" signal which are obtained by differentiating the measured voltage, $v_{c1}(t)$ and $v_{c2}(t)$. In addition, relative differences between the measured and simulated data pairs are also demonstrated in Fig. 6. The results presented in Fig. 6 correspond to test 5 of Table 5. It can be observed from Fig. 6 that the estimated signal (dotted line) is close to the measured one (solid line). In fact, the MSE values based on these plots are $\mathrm{MSE}_1 = 5.09\%$ and $\mathrm{MSE}_2 = 1.55\%$. These low MSE values (together with other four pairs of MSE values listed in Table 5) confirm the reliability of the proposed method in estimating equivalent damping parameters from the real system.

5. Conclusion

In this paper, the energy-dissipation method is extended to identify damping parameters from multi-dof vibration systems. To derive the identification algorithms, the input energy is balanced against the energy dissipated by a theoretical model, consisting of viscous and Coulomb friction. Through numerical investigations, the method has been shown to be effective and reliable in estimating equivalent damping parameters for multi-dof vibration systems no matter whether the data are noise-free or contaminated.

According to the numerical studies performed on periodic excitation, the mixed-frequency harmonic excitation is preferable to the single-frequency one. Moreover, when noise is present in the measurements, increasing the length of integration interval can be a remedy for effects of noise on estimation accuracy. Observations made on numerical study also indicate that the periodic excitation may not be the best choice. In fact, estimation results obtained from the band-limited white-noise input are more accurate than those obtained from the periodic one. Such excitations are therefore adopted in the experimental study in which an electrical system is investigated. The experimental results illustrate the reliability and applicability of the

proposed method in handling the real situations. The robustness of the method is specially tested during the experimental studies because digital differentiation and low-pass filtering are both involved.

Acknowledgements

This research is supported by National Science Council of Taiwan, under Grant no. NSC-94-2212-E-131-002. The author is indebted to Dr. Yang Liang at the Department of Mechanical Engineering of Michigan State University. Dr. Liang coincidentally has the same idea regarding how to extend the single-dof energy-dissipation method to handle multi-dof problem. The author is also indebted to Dr. Y.R. Yang at the Department of Vehicle Engineering of Mingchi University of Technology, Taiwan, who gives helpful advices on the experimental investigation.

References

[1] J.P. Den Hartog, Forced vibration with combined Coulomb and viscous damping, *Transactions of the American Society of Mechanical Engineering* 53 (1931) 107–115.
[2] M.S. Hundal, Response of a base excited system with Coulomb and viscous friction, *Journal of Sound and Vibration* 64 (1979) 371–378.
[3] J.-W. Liang, B.F. Feeny, Identifying Coulomb and viscous friction in forced dual-damped oscillators, *Journal of Vibration and Acoustics* 126 (1) (2004) 118–125.
[4] R.A. Ibrahim, Friction-induced vibration, chatter, squeal, and chaos: part I—mechanics of friction, friction-induced vibration, chatter, squeal, and chaos, *ASME Proceedings* DE-49 (1992) 107–121.
[5] B. Armstrong-Hélouvry, P. Dunpont, C. Canudas De Wit, A survey of models, analysis tools and compensation methods for the control of machines with friction, *Automatica* 30 (7) (1994) 1083–1138.
[6] J.T. Oden, J.A.C. Martins, Models and computational methods for dynamic friction phenomena, *Computer Mechanics in Applied Mechanics and Engineering* 52 (1–3) (1985) 527–634.
[7] J.-W. Liang, B.F. Feeny, Dynamical friction behavior in a forced oscillator with a compliant contact, *Journal of Applied Mechanics* 65 (1) (1998) 250–257.
[8] N. Hinrichs, M. Osetreich, K. Popp, On the modeling of friction oscillator, *Journal of Sound and Vibration* 216 (3) (1998) 435–459.
[9] D.A. Haessig, B. Friedland, On the modeling and simulation of friction, *Journal of Dynamic Systems, Measurement and Control* 113 (1991) 354–362.
[10] J.-W. Liang, B.F. Feeny, Balancing energy to estimate damping parameters in forced oscillators, *Journal of Sound and Vibration* 295 (2006) 988–998.
[11] K.S. Mohammad, K. Worden, G.R. Tomlinson, Direct parameter estimation for linear and non-linear structures, *Journal of Sound and Vibration* 152 (3) (1992) 471–499.
[12] Q. Chen, G.R. Tomlinson, Parametric identification of systems with dry friction and non-linear stiffness using a time series model, *Journal of Vibration and Acoustics* 118 (1996) 252–263.
[13] R. Ghanem, F. Romeo, A wavelet-based approach for model and parameter identification of non-linear systems, *International Journal of Non-Linear Mechanics* 36 (2001) 835–859.
[14] W.T. Thomson, M.D. Dahleh, Theory of Vibration with Applications, Prentice-Hall, Englewood Cliffs, NJ, 1998.
[15] P. Bogacki, L.F. Shampine, A 3(2) pair of Runge–Kutta formulas, *Applied Mathematics Letters* 2 (1989) 1–9.
[16] H.K. Khalil, Nonlinear Systems, Prentice-Hall, Englewood Cliffs, NJ, 1996.
[17] N.S. Nise, Control System Engineering, Wiley, New Jersey, 2000.